OPEN

Citation: Cell Death and Disease (2013) 4, e848; doi:10.1038/cddis.2013.339

www.nature.com/cddis

Loss of TAK1 increases cell traction force in a ROS-dependent manner to drive epithelial–mesenchymal transition of cancer cells

CRI Lam[1], C Tan[1], Z Teo[1], CY Tay[1], T Phua[1], YL Wu[2,3], PQ Cai[2], LP Tan[2], X Chen[2], P Zhu[1] and NS Tan*[,1,4]

Epithelial–mesenchymal transition (EMT) is a crucial step in tumor progression, and the TGFβ–SMAD signaling pathway as an inductor of EMT in many tumor types is well recognized. However, the role of non-canonical TGFβ–TAK1 signaling in EMT remains unclear. Herein, we show that TAK1 deficiency drives metastatic skin squamous cell carcinoma earlier into EMT that is conditional on the elevated cellular ROS level. The expression of TAK1 is consistently reduced in invasive squamous cell carcinoma biopsies. Tumors derived from TAK1-deficient cells also exhibited pronounced invasive morphology. TAK1-deficient cancer cells adopt a more mesenchymal morphology characterized by higher number of focal adhesions, increase surface expression of integrin $\alpha5\beta1$ and active Rac1. Notably, these mutant cells exert an increased cell traction force, an early cellular response during TGFβ1-induced EMT. The mRNA level of ZEB1 and SNAIL, transcription factors associated with mesenchymal phenotype is also upregulated in TAK1-deficient cancer cells compared with control cancer cells. We further show that TAK1 modulates Rac1 and RhoA GTPases activities via a redox-dependent downregulation of RhoA by Rac1, which involves the oxidative modification of low-molecular weight protein tyrosine phosphatase. Importantly, the treatment of TAK1-deficient cancer cells with Y27632, a selective inhibitor of Rho-associated protein kinase and antioxidant *N*-acetylcysteine augment and hinders EMT, respectively. Our findings suggest that a dysregulated balance in the activation of TGFβ–TAK1 and TGFβ–SMAD pathways is pivotal for TGFβ1-induced EMT. Thus, TAK1 deficiency in metastatic cancer cells increases integrin:Rac-induced ROS, which negatively regulated Rho by LMW-PTP to accelerate EMT.

Cell Death and Disease (2013) **4,** e848; doi:10.1038/cddis.2013.339; published online 10 October 2013
Subject Category: Cancer

Metastasis accounts for more than 90% of cancer-related deaths.[1] Metastasis is a multi-stage process involving cancer cell motility, intravasation, transit in the blood or lymph, extravasation and growth at a new site.[1] Conceivably, the various stages consist of regulatory networks with many opportunities for cancer therapy. The potential for new therapeutics avenues and their clinical impact to reduce cancer mortality rate underscores the immense importance to identify novel target modulators of these regulatory networks during metastasis.

Numerous evidences showed metastasis of epithelial cancer involve the conversion of primary cancerous epithelial cells to a migratory form, that is, undergoes epithelial–mesenchymal transition (EMT) for their dissemination to secondary tumor sites.[2] It is a process whereby cobble-stone-shaped epithelial cell colonies acquire distinct mesenchymal traits such as the loss of E-cadherin and the upregulation of N-cadherin to weaken cell–cell junctional adhesion, augmenting cell dissociation.[2] EMT also exhibit extensive cytoskeletal remodeling, whereby actin stress fibers are formed in conjunction with an increased establishment of integrin-containing focal contacts, effectively enhancing cell attachment to the extracellular matrix. Cancer cells under-going EMT are also enriched with mesenchymal type intermediate filaments (i.e. desmin, vimentin). The expression of mesenchymal features and suppression of epithelial traits are induced by early EMT-associated transcriptional factors such as SNAIL and ZEB1. Studies suggested that this mesenchymal transformation enhances the ability of cancer cells to intravasate and disseminate. Thus, the identification of mechanistic drivers of EMT would provide crucial insights and therapeutic targets to halt cancer spreading.

There are many evidences that clearly support a tumor-promoting role of inflammation in the development and progression of epithelial cancer.[3] Data from various animal models clearly emphasize that the tumor-promoting micro-environment is indispensable for tumor formation and progression. Although EMT culminates from an integrated

[1]School of Biological Sciences, Nanyang Technological University, 60 Nanyang Drive, Singapore; [2]School of Materials Science and Engineering, Nanyang Technological University, 50 Nanyang Avenue, Singapore; [3]School of Pharmaceutical Science, Xiamen University, Xiamen, China and [4]Institute of Molecular and Cell Biology, 61 Biopolis Drive, Proteos, Singapore
*Corresponding author: NS Tan, School of Biological Sciences, Nanyang Technological University, 60 Nanyang Drive, Singapore 637551, Singapore. Tel: +65 6316 2941; Fax: +65 6791 3856; E-mails: nstan@ntu.edu.sg or nstan@imcb.a-star.edu.sg
Keywords: reactive oxygen species; cell traction force; epithelial–mesenchymal transition
Abbreviations: $A5RT3_{CTRL}$, control- knockdown A5RT3 cancer cells; $A5RT3_{TAK1}$, TAK1-knockdown A5RT3 cancer cells; CAFs, cancer-associated fibroblasts; CTF, cell traction force; EMT, epithelial–mesenchymal transition; NFκB, nuclear factor kappa B; PLA, Proximity ligation assay; PNS, perilesional normal skin; qPCR, quantitative PCR; ROS, reactive oxygen species; SCC, squamous cell carcinomas; TGFβ, transforming growth factor-β; TAK1, TGFβ activated kinase 1
Received 19.2.13; revised 23.8.13; accepted 25.8.13; Edited by A Finazzi-Agró

cascade of proinflammatory cytokines, much more remains to be understood about the intracellular signaling pathways that were essential for EMT. Of the numerous cytokines produced at the tumor microenvironment, transforming growth factor-β (TGFβ) has the broadest effects, influencing many aspects of tumorigenesis.[4] TGFβ has a leading role in eliciting inflammation, serving as a chemotactic factor to recruit immune cells. TGFβ triggers EMT in tumor cells through the canonical Smad signaling.[5,6] TGFβ also signals through the non-canonical TGFβ activated kinase 1 (TAK1) cascade, which is a pivotal proinflammatory signaling mediator. However, the role of TGFβ-mediated TAK1 signaling in EMT is unclear. A hallmark of inflammation is an increase in reactive oxygen species (ROS), which also has a protumorigenic role.[7,8] TAK1 has been shown to modulate ROS level in normal and tumor cells. The ablation of TAK1 causes accumulation of ROS, resulting in epithelial cell death and inflammation.[9,10] However, the effect of ROS on EMT is not well understood. In this study, we investigated the role of TAK1 in TGFβ-induced EMT of tumor cells. We found that TAK1 deficiency in tumor cells accelerated EMT in ROS-dependent manner, thus providing a previously unexplored mechanistic regulation of EMT by TAK1.

Results

Reduced expression of TAK1 in invasive human squamous cell carcinomas (SCC). To assess the clinical relevance of TAK1, we examined the expression of TAK1 from 15 clinically graded SCCs. Tumors were formerly graded by in-house pathologist for their invasiveness, and were grouped into benign or invasive group. We observed reduced mRNA and protein levels of TAK1 in invasive SCCs when compared with its perilesional normal skin (PNS), which served as cognate-paired control. No difference was observed between benign SCCs and its corresponding PNS (Figures 1a and b). This observation suggests reduced TAK1 expression is associated with an invasive prognosis.

TAK1-deficient A5RT3 cells form skin tumors with invasive morphology. Next we set out to investigate the *in vivo* effect of TAK1 deficiency on tumor invasiveness by using SSC orthotopic nude mice model. In the first instance, we suppressed TAK1 expression in human SCC A5RT3 cell line using lentiviral-mediated RNAi (designated herein A5RT3$_{TAK1}$). A5RT3 cells transduced with a scrambled sequence served as the control A5RT3$_{CTRL}$. The efficiency of TAK1-knockdown was verified with immunoblotting and quantitative PCR (qPCR) (Supplementary Figure S1A). Immunoblot analysis of A5RT3$_{TAK1}$ cells further revealed that diminished TAK1 corresponded with a reduced downstream phosphorylation of nuclear factor kappa B (NFκB) upon treatment with interleukin-1 (IL-1)[4] (Supplementary Figure S1B). The activation of other stress response pathways like ERK and JNK were likewise also found to be suppressed in A5RT3$_{TAK1}$ (Supplementary Figure S1C). A5RT3$_{CTRL}$ and A5RT3$_{TAK1}$ cells showed no significant difference in their rate of proliferation (Supplementary Figure S1D). A5RT3$_{TAK1}$ and A5RT3$_{CTRL}$ were injected subcutaneously into nude mice to induce tumor formation. A5RT3$_{TAK1}$- and A5RT3$_{CTRL}$-derived tumors were harvested and sections were immunostained for laminin-332, a recognized marker of tumor invasiveness.[11–13] Laminin-332 immunostaining in A5RT3$_{CTRL}$-derived tumors appeared as demarcated boundaries characteristic of basement membrane type architecture, whereas the corresponding staining in A5RT3$_{TAK1}$-derived tumors was disorganized and interspersed among the tumor epithelial cells, indicative of enhanced invasiveness. This spatial disparity in laminin-332 immunostaining also corresponded with an increased laminin-332 protein (Figure 1d). Gelatin zymography also revealed increased MMP-9 activity, another marker of tumor invasiveness, in A5RT3$_{TAK1}$-tumor. These observations indicate that the TAK deficiency is associated with enhanced invasiveness (Figure 1d).

TAK1 deficiency promotes TGFβ-1 induced EMT in A5RT3 cells. Reduced TAK1 expression is a common attribute of invasive human SCCs. In addition, TAK1-deficient tumors exhibited more prominent invasive features. The TGFβ1–SMAD signaling pathway is central to EMT induction. However, the role of TGFβ1–TAK1 signaling in EMT remains unknown. A5RT3$_{TAK1}$ colonies treated with TGFβ1 showed earlier separation at cell–cell borders at 48 h post treatment (Figure 1e). Immunofluorescence staining revealed a decreased E-cadherin and a corresponding increased N-cadherin staining (Figure 1f). The mRNA levels of EMT markers measured by qPCR revealed an EMT phenotype as early as 24 h after exposure in A5RT3$_{TAK1}$ treated with TGFβ compared with cognate controls (Figure 1g). The protein expression of EMT markers vimentin, fibronectin, Snail 1 and Snail 2 was also altered, indicating an earlier switch to an EMT phenotype by A5RT3$_{TAK1}$ cells (Figure 1h). To further assess the potential role of TAK1 in EMT, we examined TGFβ1-induced EMT in three other tumor lines, HSC-5, II4 and MKN28, whose endogenous TAK1 was suppressed by siRNA. HSC-5 was established from a clinically derived human squamous cell carcinoma.[14] II4 cell line is a Ras-transformed HaCat cell line that is not metastatic.[15] MKN28 is a well-differentiated stomach adenocarcinoma cell line.[16] Importantly, we also observed similar augmentation of TGFβ1-induced EMT in these TAK1-knockdown cells. TAK1-deficient cells were observed to adopt mesenchymal-like cell–cell separation upon TGFβ1 induction (Supplementary Figure S1E) and corresponded to the expression of mesenchymal markers (Supplementary Figure S1F). These observations support a role of TAK1 deficiency in promoting mesenchymal transition. We also found that TGFβ-induced EMT phenotype was prevented in A5RT3$_{TAK1}$ transfected with an expression vector for TAK1 pCDNA–TAK1 (Supplementary Figure S2). The TAK1 mRNA sequence transcribed from pCDNA–TAK1 contains silent mutations that are not targeted by the siRNA produced in A5RT3$_{TAK1}$.

To understand the relationship between SMAD and TAK1 in TGFβ1-induced EMT, we assessed the relevance of SMAD3 in TGFβ1-induced EMT of A5RT3$_{TAK1}$ cells, which was previously unclear. A5RT3$_{TAK1}$ cells were transiently transfected with siRNA targeting SMAD3 (Figure 2). Loss of SMAD3 in A5RT3$_{TAK1}$ cells inhibited TGFβ1-induced EMT

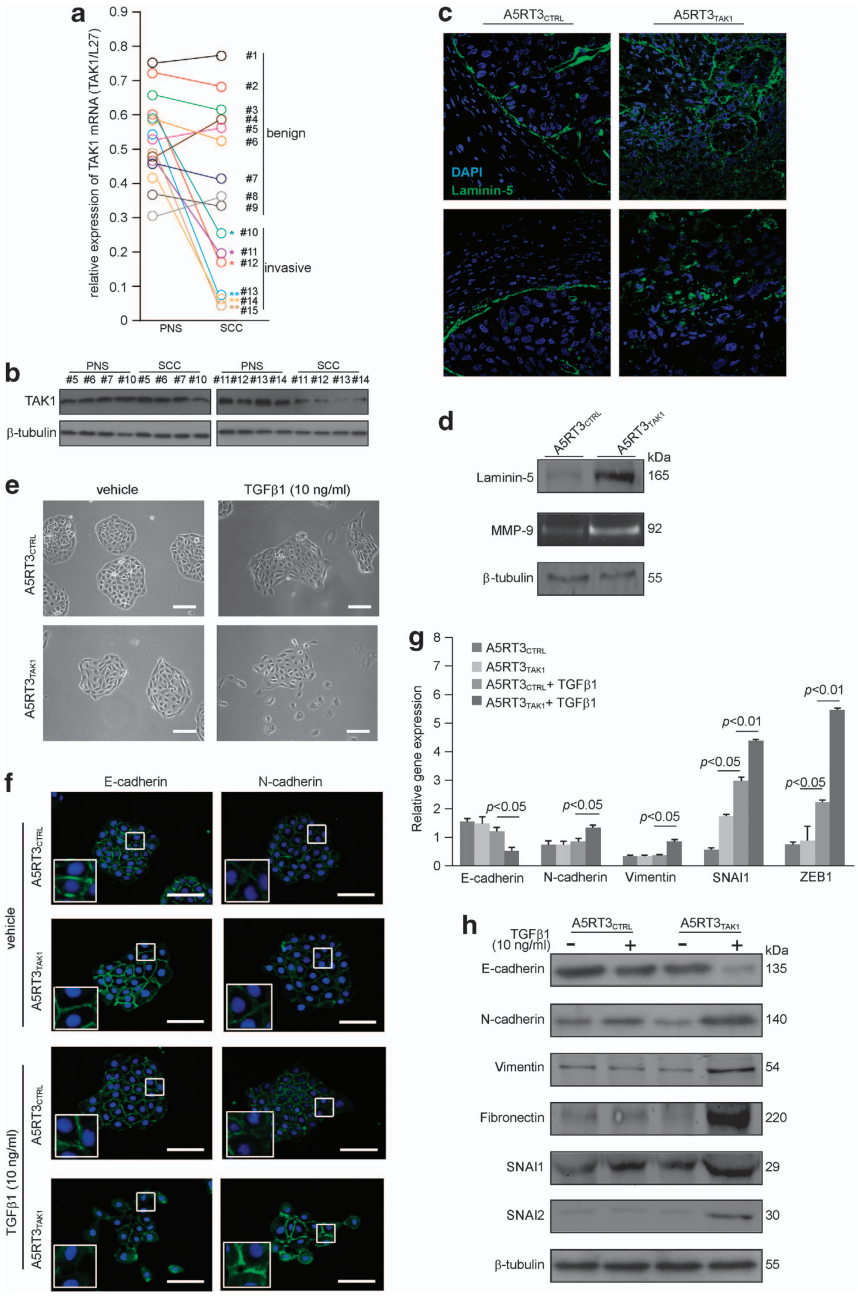

Figure 1 TAK1 deficiency promotes TGFβ1 induced EMT in A5RT3 cells. (**a** and **b**) Relative mRNA (**a**) and protein (**b**) expression of TAK1 in human squamous cell carcinomas (SCC) biopsies and their cognate perilesional normal skin (PNS). Biopsies #1–9 and #10–15 are benign and invasive grades SCC samples, respectively. Biopsies #5–7 and #10–14 were used for western blot analysis. For qPCR, data points from the same individual are linked by colored lines. (**c**) Immunofluorescence staining of laminin-332 (green) in cryosections of A5RT3$_{CTRL}$- and A5RT3$_{TAK1}$-derived tumors. Nuclei were counterstained with DAPI (blue). (**d**) Expression of invasive markers laminin-332 and MMP-9 in A5RT3$_{CTRL}$- and A5RT3$_{TAK1}$-derived tumors as determined by immunoblot and gelatin zymography, respectively. Values below each band represent the mean fold differences ($n = 3$) in expression level when compared with A5RT3$_{CTRL}$-derived tumor. (**e**) Phase-contrast microscopy images of A5RT3$_{CTRL}$ and A5RT3$_{TAK1}$ cell colonies 48 h after TGFβ1 treatment. Scale bar, 100 μm. (**f**) Immunostaining of E-cadherin and N-cadherin (green) in A5RT3$_{CTRL}$ and A5RT3$_{TAK1}$ cells under the indicated treatment. Nuclei were counterstained with DAPI (blue). Scale bar, 100 μm. (**g**) qPCR analysis of EMT markers in A5RT3$_{CTRL}$ and A5RT3$_{TAK1}$ 24 h after TGFβ1 treatment. Samples were normalized with reference gene, L27. (**h**) Representative western blots of EMT markers in A5RT3$_{CTRL}$ and A5RT3$_{TAK1}$ 48 h after TGFβ1 treatment. The densitometry values as indicated below respective lanes were normalized with respect to the control. For western blot, β-tubulin was used as a loading control. For qPCR, all samples were normalized with housekeeping gene L27 gene. Data represent means ± S.D.; $n = 3$

(Figure 2a). The expression of mesenchymal markers was downregulated whereas epithelial markers were upregulated in SMAD3-deficient A5RT3$_{TAK1}$ cells (Figures 2b and c). We observed that EMT also occurred in A5RT3$_{CTRL}$ cell colonies after prolonged (i.e. 72 h) treatment with TGFβ1 as compared to 48 h for A5RT3$_{TAK1}$ (Supplementary Figure S3A). Similarly, SMAD3 deficiency in A5RT3$_{CTRL}$ cells inhibited TGFβ1-induced EMT (Supplementary Figures S3B & S3C).

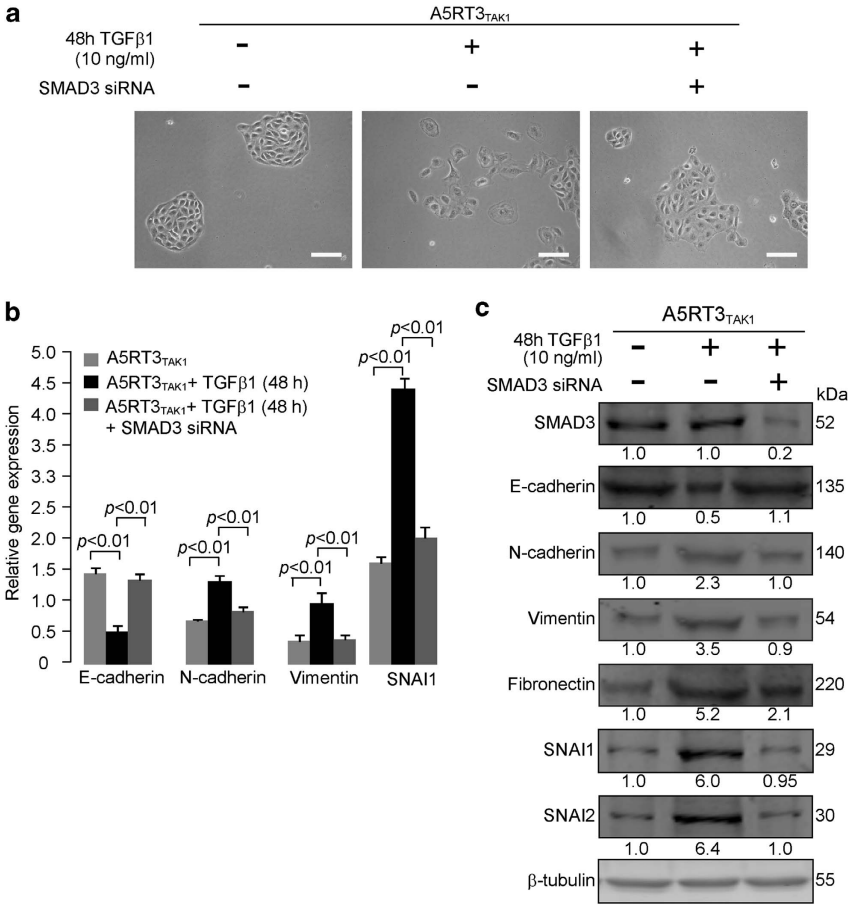

Figure 2 TGFβ1-induced EMT is effected through SMAD signaling. (**a**) Phase-contrast images of SMAD3 siRNA-transfected A5RT3$_{TAK1}$ and respective control cells with 48 h of TGFβ1 (10 ng/ml) treatment. Scale bar, 100 μm. (**b**) qPCR analysis of EMT markers in SMAD3 siRNA-transfected A5RT3$_{TAK1}$ cells with and without TGFβ1 treatment. (**c**) Immunoblot analysis of SMAD3 siRNA-transfected A5RT3$_{TAK1}$ cells for their knockdown and EMT markers upon TGFβ1 treatment. Representative blots were shown with respective densitometry values indicated below lanes, normalized with respect to the control. For western blot, β-tubulin was used as a loading control. For qPCR, all samples were normalized with housekeeping gene L27 gene. Data represent means ± S.D.; $n = 3$

The phosphorylation of SMAD3 was also evaluated in the SMAD3-knockdown cells by immunoblotting (Supplementary Figure S3D). Altogether, our observations indicates that TAK1 limits TGFβ driven pro-EMT signals mediated by SMAD3 pathway, and suggests a signaling balance between the canonical SMAD3 and non-canonical TAK1 in regulating EMT.

TAK1 deficiency increases the expression of surface integrin β1 and β3. Our above observations suggest that TAK1 deficiency in A5RT3 facilitated TGFβ1-induced EMT. EMT involves the transition of the epithelial cancer cells from predominantly cell–cell adhesion to a cell–ECM interaction. Integrins are major cell surface receptors that enable bidirectional communication between the cells with the ECM are thus well apt to influence cellular behavior involved in EMT including migration and adhesion.[17,18] Thus, we examined the surface expression of integrins β1, β3, β4, β5 and β7 on A5RT3$_{TAK1}$ (Figure 3a). We found that A5RT3$_{TAK1}$ had significantly increased surface levels of β1 and β3 integrins (Figure 3a). We further conducted staining of α5β1 integrin and found that it is also significantly elevated in a manner reminiscent of integrin β1 (Figure 3b). Proximity ligation assay (PLA) also confirmed higher level of surface α5β1 integrin in A5RT3$_{TAK1}$ than A5RT3$_{CTRL}$ (Figure 3c, upper panel). PLA assay was conducted without Triton-X permeabilization to detect only to surface integrin levels. PLA signals for integrin α5β1 were predominantly situated along the cell–cell boundary (Figure 3c, upper panel). PLA assay performed using antibody against active integrin β1 and configuration-specific monoclonal anti-Rac1-GTP antibody further confirmed that the increase expression of surface integrin was associated with an elevated Rac1 activation, suggesting a remodeling of the cytoskeleton (Figure 3c, lower panel).

Loss of TAK1 increases cell traction force in A5RT3 during EMT. During EMT, integrins are recruited to distinct contact points to form focal adhesions accompanied by cytoskeletal remodeling of cortical actin network to filamentous stress fibers. Interestingly, we already observed more focal adhesions and better developed stress fiber formation in A5RT3$_{TAK1}$ than A5RT3$_{CTRL}$, before TGFβ1 treatment (Figure 4a). These differences in stress fiber formation correlated with vinculin-positive focal adhesion staining at their cell junctions of A5RT3$_{TAK1}$ (Figure 4a). The vinculin

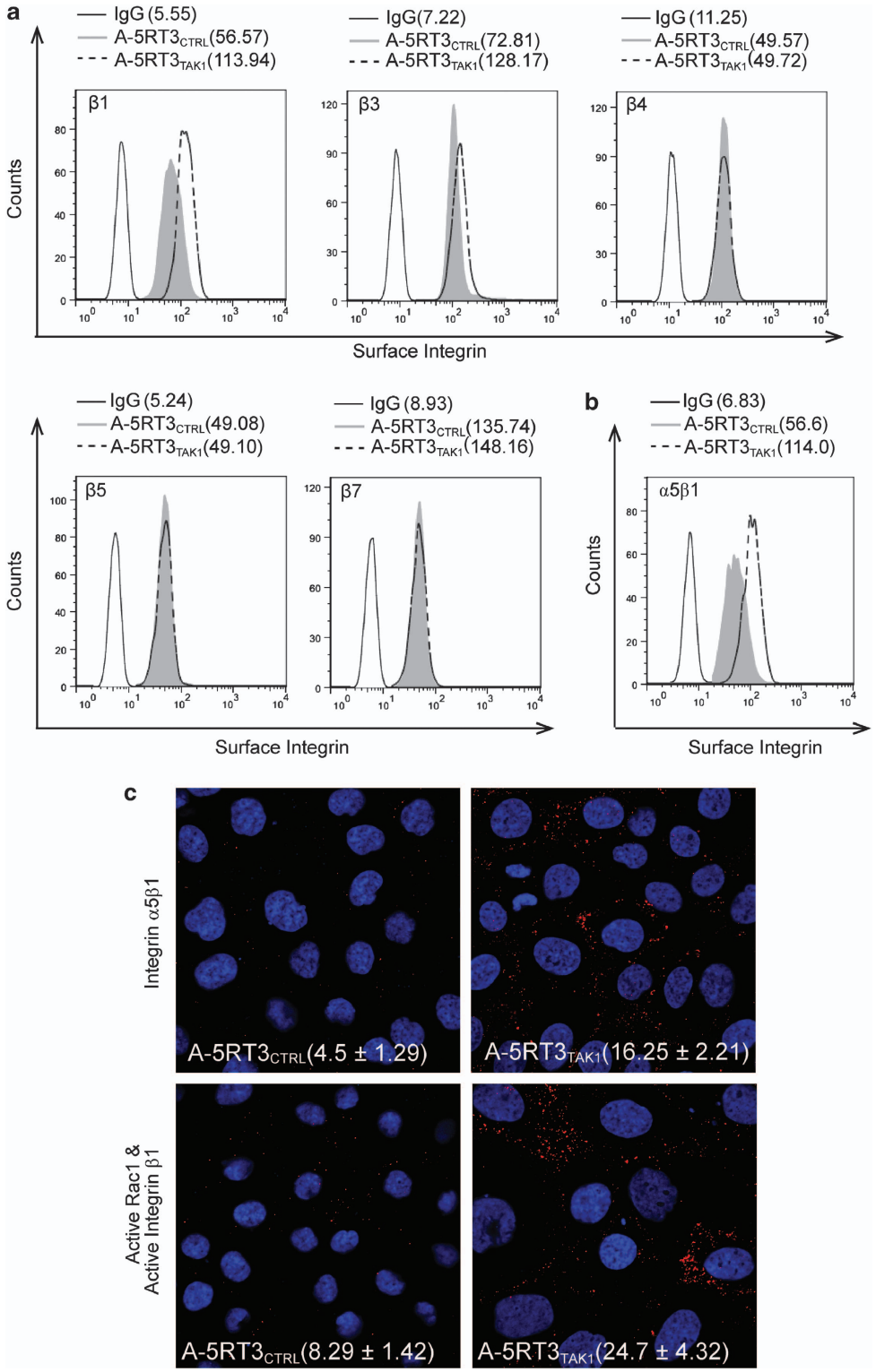

Figure 3 Expression of surface integrin in A5RT3$_{CTRL}$ and A5RT3$_{TAK1}$. (**a** and **b**) FACS analysis of A5RT3$_{CTRL}$ and A5RT3$_{TAK1}$ cells immunostained with antibodies against indicated surface integrin β subunits (**a**) and with integrin α5β1 (**b**). The distribution of tumor cells with regard to their extent of integrin staining was presented in histogram plots with the identity of the stained integrin subunit indicated (top left). Cells stained with only control IgG served as the negative controls. Each image is representative of at least three different experiments. Values shown indicate mean fluorescence intensity. (**c**) PLA assay of α5β1 integrin expression (upper panel) and active integrin β1:active Rac1 (lower panel) n A5RT3$_{CTRL}$ and A5RT3$_{TAK1}$ cells. Representative images were shown with mean number of PLA spots per nucleus ± S.D. indicated; $n = 3$

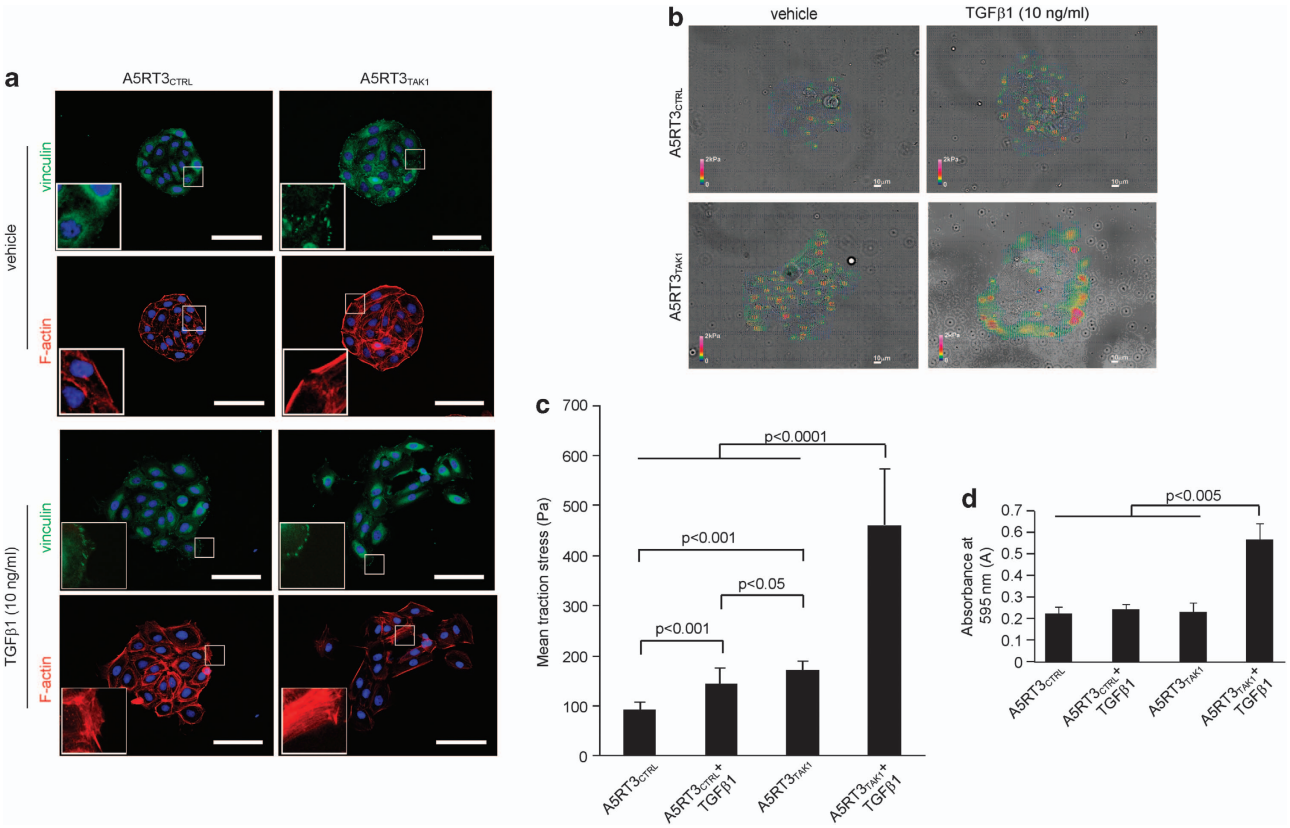

Figure 4 TAK1 deficiency increases cell traction force in A-5RT3 facilitating EMT. (**a**) Vinculin immunostaining (green) and phalloidin F-actin (red) staining were conducted of $A5RT3_{CTRL}$ and $A5RT3_{TAK1}$ cell colonies with and without TGFβ1 treatment for 48 h with representative images shown. Scale bar, 100 μm. (**b** and **c**) Cell traction force profiling (**b**) and mean measured cell traction stress (**c**) of $A5RT3_{CTRL}$ and $A5RT3_{TAK1}$ with and without TGFβ1 (10 ng/ml) treatment for 24 h. Color scale bar denotes traction stress (kPa). Scale bar, 10 μm. Values (mean + S.D.) of three independent measurements. (**d**) $A5RT3_{CTRL}$ and $A5RT3_{TAK1}$ cells were seeded on a transwell membrane of pore size and evaluated for their migration through the pore with and without TGFβ1 treatment for 48 h. Migrated cells were stained with crystal violet and destained with a fixed volume of 0.5% Triton-X solution. Absorbance at 595 nm of the solutions was measured to quantify transwell migration. Graph displays mean absorbance values ± S.D.; $n = 3$

staining also displayed differences in spatial distribution observed in PLA staining for integrin $\alpha5\beta1$. As expected, the treatment with TGFβ1 increased stress fiber in both cell lines despite their different cell–cell dispersion. Differences in stress fibers and focal adhesion contact formation in cells are known to effect differential cell traction force (CTF) generation. These force differences represent the early detectable changes in cell responses, preceding the appearance of visible morphological changes. Thus, we measured the CTF generated in $A5RT3_{TAK1}$ and $A5RT3_{CTRL}$ using CTF microscopy. Cells were cultured on fibronectin-treated compliant PDMS substrate (10 kPa) coated with a monolayer of fluorescence beads. Traction force is determined by measuring the displacement of the fluorescence beads in the *x-y* plane because of the contraction exerted by the cell. Notably, $A5RT3_{TAK1}$ generated a considerably different CTF profile from that of control $A5RT3_{CTRL}$ cells. Although traction field was observed to be concentrated along the periphery of the $A5RT3_{CTRL}$ cell colony, intra-colony traction can only be detected in the $A5RT3_{TAK1}$ group (Figure 4b). As the CTF exerted is also relative to the cell colony size and shape, measured CTF values are divided over the area covered by the cell colonies to derive traction stress values for comparison between cell colonies of differing sizes. Untreated $A5RT3_{CTRL}$ cells displayed a mean traction stress value of 93.4 ± 14.8 Pa, whereas that of $A5RT3_{TAK1}$ displayed a mean CTF of 170.7 ± 20.2 Pa (Figure 4c), indicating higher contractility in TAK1-deficient cancer cells. TGFβ1 induction resulted in significant CTF increments for both $A5RT3_{CTRL}$ and $A5RT3_{TAK1}$ as reflected in their elevated traction stress values of 143.96 ± 31.7 Pa and 461.4 ± 113.22 Pa, respectively (Figure 4c). Notably, TGFβ1-induced $A5RT3_{CTRL}$ cell colonies also adopted a CTF profile pattern comparable with that of untreated $A5RT3_{TAK1}$. In transwell invasion assay, we found that $A5RT3_{TAK1}$ significantly migrated faster through an 8-μm pore transwell with TGFβ1 as the chemotactic factor (Figure 4d). Our results indicate that TAK1 deficiency in A5RT3 promoted the expression of $\beta1$ and $\beta3$ integrins, and altered stress fiber formation. This cytoskeletal remodeling corresponded with an increased CTF profile and metastatic potential in $A5RT3_{TAK1}$ cells, suggesting an inhibitory role of endogenous TAK1 during TGFβ1-induced EMT.

Elevated ROS levels in TAK1-deficient tumor cells accelerate EMT. TAK1 deficiency was reported to upregulate ROS level in human keratinocytes and in cancer cells.[9,19] Integrin-Rac1 signaling mediates multiple pathways

that control actin cytoskeletal changes, transcriptional activity and ROS production.[20,21] First, we examine if the increased active Rac1 in A5RT3$_{TAK1}$ (Figure 3c) was associated with a higher recruitment of Rac1-dependent Nox1 for ROS generation. PLA assay using antibodies against active Rac1 and Nox1 revealed higher number of PLA signals in A5RT3$_{TAK1}$ than A5RT3$_{CTRL}$, indicating an elevated Rac1-dependent activation of Nox1 (Figure 5a). Next, we evaluated intracellular ROS production in A5RT3$_{TAK1}$ and A5RT3$_{CTRL}$ using fluorescence dye CM-H2DCFDA followed by FACS analysis. We found that A5RT3$_{TAK1}$ cells have increased ROS level, which was further potentiated by TGFβ1 induction. In fact, the ROS level in untreated A5RT3$_{TAK1}$ was comparable with TGF-β1-treated A5RT3$_{CTRL}$ (Figure 5b). The difference in ROS level between A5RT3$_{CTRL}$ and A5RT3$_{TAK1}$ upon TGFβ1 treatment was also verified by fluorescence microscopy. Interestingly, we observed that A5RT3$_{TAK1}$ cells that have separated from the tumor colony were more intensely stained with CM-H2DCFDA compared with A5RT3$_{CTRL}$ (Figure 5c). As ROS upregulation in A5RT3$_{TAK1}$ correlated with the mesenchymal phenotype induced by TGFβ1, it was conceivable that the observed elevated oxidative stress may be mechanistically involved in EMT. Antioxidant *N*-acetylcysteine (NAC) addition was utilized to quench ROS. First, we determine the optimal concentration of NAC (30 μM–30 mM) for our experiments. At NAC concentrations of 3–30 mM, annexin V/propidium iodide staining of A5RT3$_{TAK1}$ revealed increased percentage of apoptotic cells (Supplementary Figure S4A). A corresponding CM-H2DCFDA staining showed that the ROS level was increased in cells treated with high 30 mM NAC concentration, most likely due to cell death. The treatment with 300 μM–3 mM of NAC did not lower the ROS further than that obtained by 100 μM of NAC. At 30 μM of NAC, the decrease in ROS was less effective (Figure 4b). Thus, we determine the optimal NAC concentration to be 100 μM, which lowers the ROS level without substantially increasing cell death. We quenched the ROS in the cancer cells with NAC and observed that the treatment hindered the cell–cell separation characteristic of TGFβ1-induced EMT in A5RT3$_{TAK1}$ (Figure 5d). The NAC-treated cells were significantly diminished of their EMT traits (Figures 5e and f). NAC treatment neither altered the phenotype of A5RT3$_{CTRL}$ cells (Supplementary Figure S4C) nor elicited any off-target effects as verified by immunoblotting of various EMT markers (Supplementary Figure S4D).

Inhibition of Rho accelerated TGFβ1-induced EMT in A5RT3$_{TAK1}$. Our above observations on increased CTF of untreated A5RT3$_{TAK1}$ corresponded with the increased surface integrin expression, focal adhesion and stress fiber formation. RhoA and Rac1 have key roles in the formation of stress fiber, focal adhesion, cytoskeleton organization and cellular migration. We first examined their activities in A5RT3$_{CTRL}$ and A5RT3$_{TAK1}$ with and without TGFβ1 induction. In both TGFβ1-treated and -untreated groups, the activities of Rac1 and RhoA were elevated and reduced, respectively, in A5RT3$_{TAK1}$ compared with A5RT3$_{CTRL}$ (Figure 6a). We observed that NAC treatment increased RhoA activity, but has not significantly affected the level of active Rac1 (Figure 6a). This is consistent with our earlier observation that increased surface expression of integrin β1 activated Rac1, which subsequently engaged Nox1 for ROS generation. It also suggested that the activity of RhoA was redox-dependent. To further understand the relationship between Rac1 and ROS, we transfected A5RT3$_{CTRL}$ and A5RT3$_{TAK1}$ with expression vectors containing constitutively active (G12V) and dominant-negative Rac mutant (T17N), respectively. FACS analysis revealed that A5RT3$_{CTRL}$(G12V) cells have increased ROS content compared with control vector transfected A5RT3$_{CTRL}$ (Figure 6b). Conversely, the oxidative stress level of A5RT3$_{TAK1}$(T17N) was significantly decreased compared with A5RT3$_{TAK1}$ (Figure 6b). In contrast to their cognate parent cell lines, A5RT3$_{CTRL}$(G12V) and A5RT3$_{TAK1}$(T17N) showed increased and reduced TGFβ1-induced EMT, respectively (Figure 6c).

To understand how ROS can modulate the activity of RhoA, we employed the sensitive cysteine-targeted biotin switch method to label oxidatively modified proteins. We showed that the oxidation of low-molecular weight protein tyrosine phosphatase (LMW-PTP), a potential downstream target of ROS was significantly increased in A5RT3$_{TAK1}$. LMW-PTP oxidation was, however, undetectable in NAC-treated A5RT3$_{TAK1}$ cells (Figure 6a) regardless of TGFβ1 treatment. Oxidatively modified LMW-PTP has been shown to inhibit RhoA activity.[20] To understand the role of RhoA in TGFβ1-induced EMT, we treated A5RT3$_{TAK1}$ with Y27632, a selective inhibitor of Rho-associated protein kinase, the downstream mediator of RhoA. The inhibition of Rho augmented EMT in A5RT3$_{TAK1}$ cells detected within 24 h post-TGFβ1 treatment (Figure 6d). The Y27632-treated cells had decreased epithelial marker expression and increased expression of mesenchymal markers (Figure 6e). To further confirm the role of RhoA in attenuating EMT, we transfected A5RT3$_{TAK1}$ cells with RhoA siRNA and observed an increase EMT-like dispersion (Figure 6d). These RhoA-knockdown cells also exhibited changes in the expression of EMT markers (Figure 6e). The inhibition of ROCK and the suppression of RhoA by siRNA in A5RT3$_{CTRL}$ also stimulated the expression of EMT markers, albeit at a reduced level (Supplementary Figure S5). Altogether, our observations showed that TAK1 deficiency increased integrin:Rac1-induced ROS, which negatively regulated RhoA by LMW-PTP to accelerate EMT.

Discussion

Chronic inflammation has been linked to various steps involved in tumorigenesis, including cellular transformation, promotion, invasion and metastasis.[22,23] Among the numerous cytokines involved in inflammation and tumorigenesis, TGFβ1 has the broadest effect, influencing cell growth, cancer invasion and spreading.[24,25] Cellular response to TGFβ1 is cell-type specific and context-dependent. EMT is a crucial step in tumor progression, and the TGFβ-SMAD signaling pathway as an inductor of EMT in many tumor types is well-recognized.[26,27] However, the role of TGFβ–TAK1 signaling in EMT remains unclear. Earlier studies showed that TAK1 through the NFκB signaling pathway triggered increased EMT and invasiveness in tumor.[28] Recent studies also

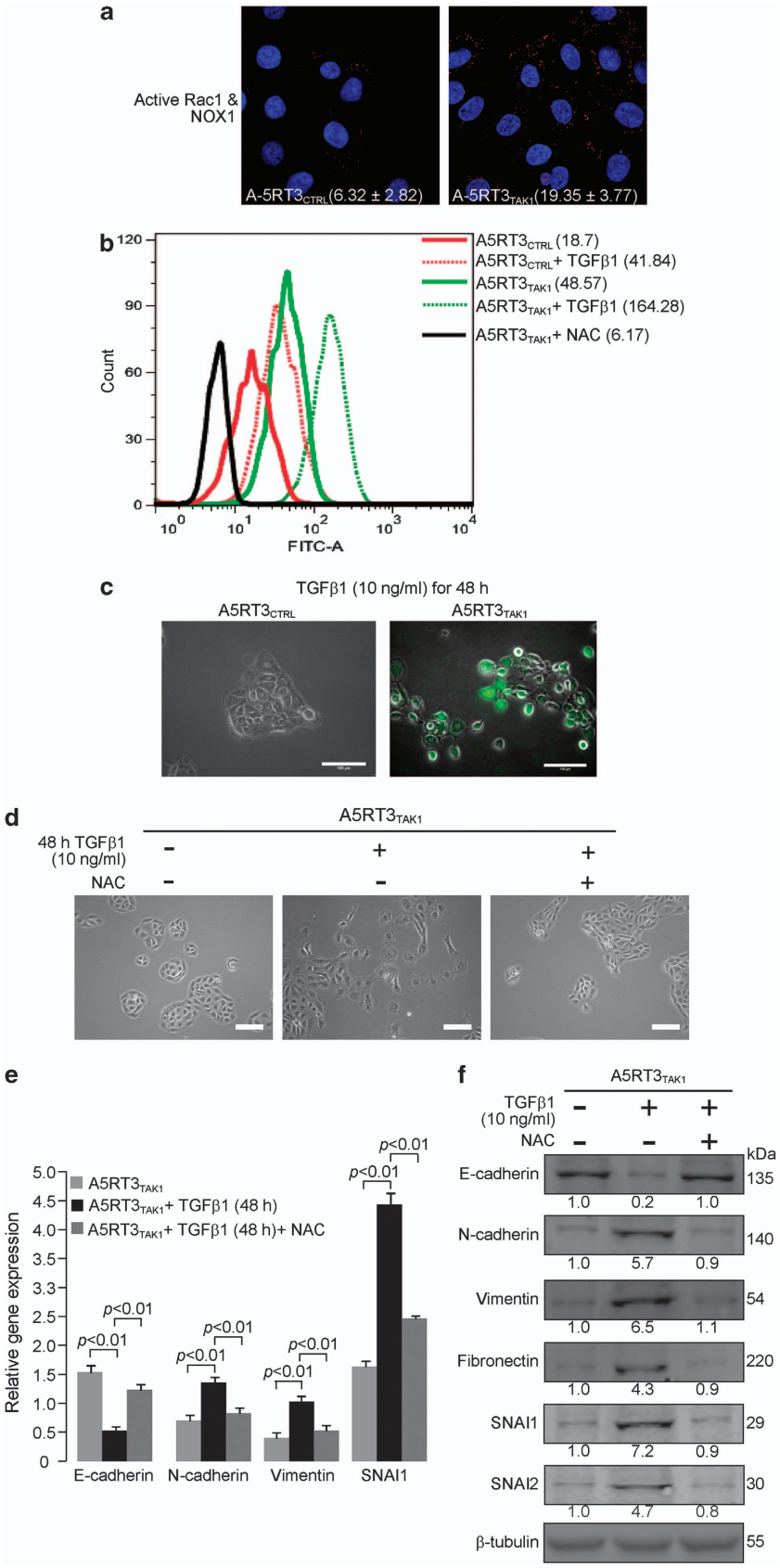
a
Active Rac1 & NOX1
A-5RT3CTRL(6.32 ± 2.82)
A-5RT3TAK1(19.35 ± 3.77)
b
A5RT3CTRL (18.7)
A5RT3CTRL+ TGFβ1 (41.84)
A5RT3TAK1 (48.57)
A5RT3TAK1+ TGFβ1 (164.28)
A5RT3TAK1+ NAC (6.17)
Count
FITC-A
c
TGFβ1 (10 ng/ml) for 48 h
A5RT3CTRL
A5RT3TAK1
d
A5RT3TAK1
48 h TGFβ1 (10 ng/ml)
NAC
e
A5RT3TAK1
A5RT3TAK1+ TGFβ1 (48 h)
A5RT3TAK1+ TGFβ1 (48 h)+ NAC
Relative gene expression
p<0.01
E-cadherin
N-cadherin
Vimentin
SNAI1
f
A5RT3TAK1
TGFβ1 (10 ng/ml)
NAC
kDa
E-cadherin 135
1.0 0.2 1.0
N-cadherin 140
1.0 5.7 0.9
Vimentin 54
1.0 6.5 1.1
Fibronectin 220
1.0 4.3 0.9
SNAI1 29
1.0 7.2 0.9
SNAI2 30
1.0 4.7 0.8
β-tubulin 55

implicated ROS-mediated oxidative stress to promote tumorigenesis[29] Herein, we found that squamous cell carcinoma progressed earlier into EMT that was conditional on elevated cellular ROS level resulting from TAK1 deficiency (Figure 7). Notably, the expression of TAK1 was consistently reduced in invasive SCCs, but not in benign SCCs, when compared with their cognate perilesional normal tissues. Furthermore, tumors derived from TAK1-deficient cells expressed elevated levels of MMP-9 and laminin-332, the latter was spatially dispersed in the epithelial tumor region. Our investigation further showed that TAK1-deficient cancer cells exhibited an increased cell traction force, one of the earliest cellular response during EMT.[30,31] This cellular response was associated with an increase in surface integrin $\alpha5\beta1$, a well-known mesenchymal marker in cancer.[32] We found increased active integrin and active Rac1 interactions in TAK1-deficient cancer cells. The elevated active Rac1 mediated the recruitment of Rac-dependent Nox1 and higher ROS production. Rac1-mediated ROS production resulted in the downregulation of Rho activity in TAK1-deficient cancer cells. The redox-dependent decrease in Rho activity was required for Rac1-induced formation of integrin-mediated cell spreading during TGFβ1-induced EMT. Conversely, the suppression of Rac1 hindered the progression of EMT by TAK1-deficient cancer cells. The redox-dependent downregulation of RhoA involves the inhibition of LMW-PTP.[20] Thus, TAK1 modulates Rac1 and Rho GTPases activities, which are critical regulators of actin cytoskeleton remodeling during EMT.

Numerous studies have revealed a biphasic role of epithelial TGFβ1 signaling in tumorigenesis, but our molecular understanding for this phenomenon remains unclear. In the early stages of cancer, TGFβ1 has tumor suppressive effects, whereas in the advanced stages of cancer, TGFβ1 can promote the growth of tumor cells, as well as induce EMT, which results in metastasis.[25,33] The role of TGFβ–TAK1 in tumorigenesis is only emerging. It was reported that in mouse skin tumor, the deletion of *TAK1* gene increases cellular apoptosis due to elevated ROS level.[19] In fact, TAK1-deficient cancer cells displayed increased propensity to undergo EMT upon TGFβ1 exposure. Thus, our findings together with that of others suggest that TGFβ–TAK1 signaling also exhibited a biphasic role during tumor progression. In early development of tumor, TAK1 promotes tumor growth by reining ROS production and ROS-mediated apoptosis. In advance tumor stage, TAK1 discourages EMT and thus delays metastasis. Although we observed a similar increase ROS in our TAK1-deficient cancer cells, in contrast to the mouse study,[19] no significant difference in proliferation or apoptosis were observed. This discrepancy may be due the influence of other surrounding cell types, such as cancer-associated fibroblasts (CAFs). The development and progression of neoplastic epithelia can be understood to arise from the deregulation of this dynamic interaction between normal epithelial and stromal fibroblasts.[34,35] Recent studies of TGFβ signaling in stromal fibroblasts showed significant paracrine influence on the behavior of adjacent epithelial cell. Mice with a fibroblast-specific deletion of TGFβ receptor type II developed intraepithelial neoplasia in prostate and invasive squamous cell carcinoma of the forestomach.[36,37] Clearly, a better understanding the role of TGFβ–TAK and TGFβ–SMAD signalings in CAFs, and their influence on epithelial cell behaviors requires our future attention. In summary, we showed that TAK1 deficiency increases CTF by a ROS-dependent manner to drive EMT in metastatic A5RT3 cells. Our findings suggest that a dysregulated balance in the activation of TGFβ–TAK1 and TGFβ–SMAD pathways is pivotal for TGFβ1-induced EMT.

Materials and Methods

Materials. Antibodies were purchased against integrin $\alpha5\beta1$ (Millipore, Billerica, MA, USA), TAK1, NFκBp65, phospho NFκBp65, E-cadherin, SMAD3, phospho-SMAD3, ERK, phospho-ERK, JNK, phospho-JNK (Cell Signaling, Danvers, MA, USA), Rac1, RhoA (Cytoskeleton Inc), activated RhoA, activated Rac1 (NewEast Biosciences, King of Prussia, PA, USA), vimentin, snail2 (Millipore), laminin-332 (AB14509, Abcam, Cambridge, MA, USA), N-cadherin, β-tubulin, snail1, fibronectin, Nox1 and secondary HRP-conjugated antibodies (Santa Cruz Biotechnology, Dallas, TX, USA) for immunoblotting or immunostaining. Transfection reagent ExGen 500 was purchased from Fermentas. Double-promoter lentivirus-based siRNA vector and pFIV packaging kit were acquired from System Biosciences (Mountain View, CA, USA). Pooled siRNA and transfection reagent were purchased from Dharmacon (Pittsburgh, PA, USA). All restriction enzymes and DNA/RNA-modifying enzymes were obtained from Fermentas. TGFβ1 and IL-1 were purchased from Peprotech (Rehovot, Israel). Otherwise, chemicals were purchased from Sigma-Aldrich (St. Louis, MO, USA).

Reverse-transcription and real-time PCR (qPCR). Total RNA was isolated and reverse transcribed as previously described.[9] The cDNA were used for qPCR using SYBR-Green Master mix (KAPABiosystem, Woburn, MA, USA). Melt curve analysis was included to assure that only one PCR product was formed. Expression was normalized to the control gene ribosomal L27, which did not change under any of the experimental conditions studied. Average fold change was derived from three independent experiments and two-tailed student *t*-tests were performed to evaluate statistical significance of expressional changes. The sequences of primers are in Supplementary Table S1.

Tumorigenicity assay. Primary tumor formation was monitored over a period of 2 months after subcutaneous injection of 2×10^6 tumor cells resuspended in 100 μl of DMEM medium containing Matrigel (5 mg/ml) into the interscapular region of 6-week-old BALB/c athymic nude mice. Animals were killed at tumor size of 10 mm diameter. Excised tumors were fixed in 4% paraformaldehyde overnight followed by overnight equilibration in 30% sucrose/PBS for cryoprotection before embedding and freezing in OCT medium (Tissue-tek, Alphen aan den Rijn, The Netherlands). Frozen tumor tissues were sectioned and immunostained as previously described.[38]

Figure 5 Role of elevated ROS during TGFβ1-induced EMT in A5RT3$_{TAK1}$. (**a**) PLA assay of active Rac1 and Nox1 in A5RT3$_{CTRL}$ and A5RT3$_{TAK1}$ cell. Representative images were shown with mean number of PLA spots per nucleus ± S.D. indicated; $n = 3$. (**b**) A5RT3$_{CTRL}$ and A5RT3$_{TAK1}$ with or without 48 h of TGFβ1 (10 ng/ml) treatment were stained with DCF and analyzed with flow cytometry. Antioxidant NAC-treated cells (100 μM) served as a negative control. Image shown is representative of three different experiments. Values shown indicate mean fluorescence intensity. (**c**) Phase-contrast images showing DCF staining of A5RT3$_{CTRL}$ and A5RT3$_{TAK1}$ after 48 h of TGFβ1 (10 ng/ml) treatment. Scale bar, 100μm. (**d**) Phase-contrast images A5RT3$_{TAK1}$ cells subjected to indicated treatements. NAC (100 μM) was used to quench ROS. Scale bar, 100 μm. (**e**) qPCR analysis of EMT markers in TGFβ1 induced A5RT3$_{TAK1}$ with NAC treatment. Samples were normalized with reference gene, L27. (**f**) Representative blots of EMT markers in TGFβ1 induced A5RT3$_{TAK1}$ with NAC treatment were shown with densitometry values indicated below respective lanes. Samples were normalized with tubulin as a loading control. Data represent means ± S.D.; $n = 3$

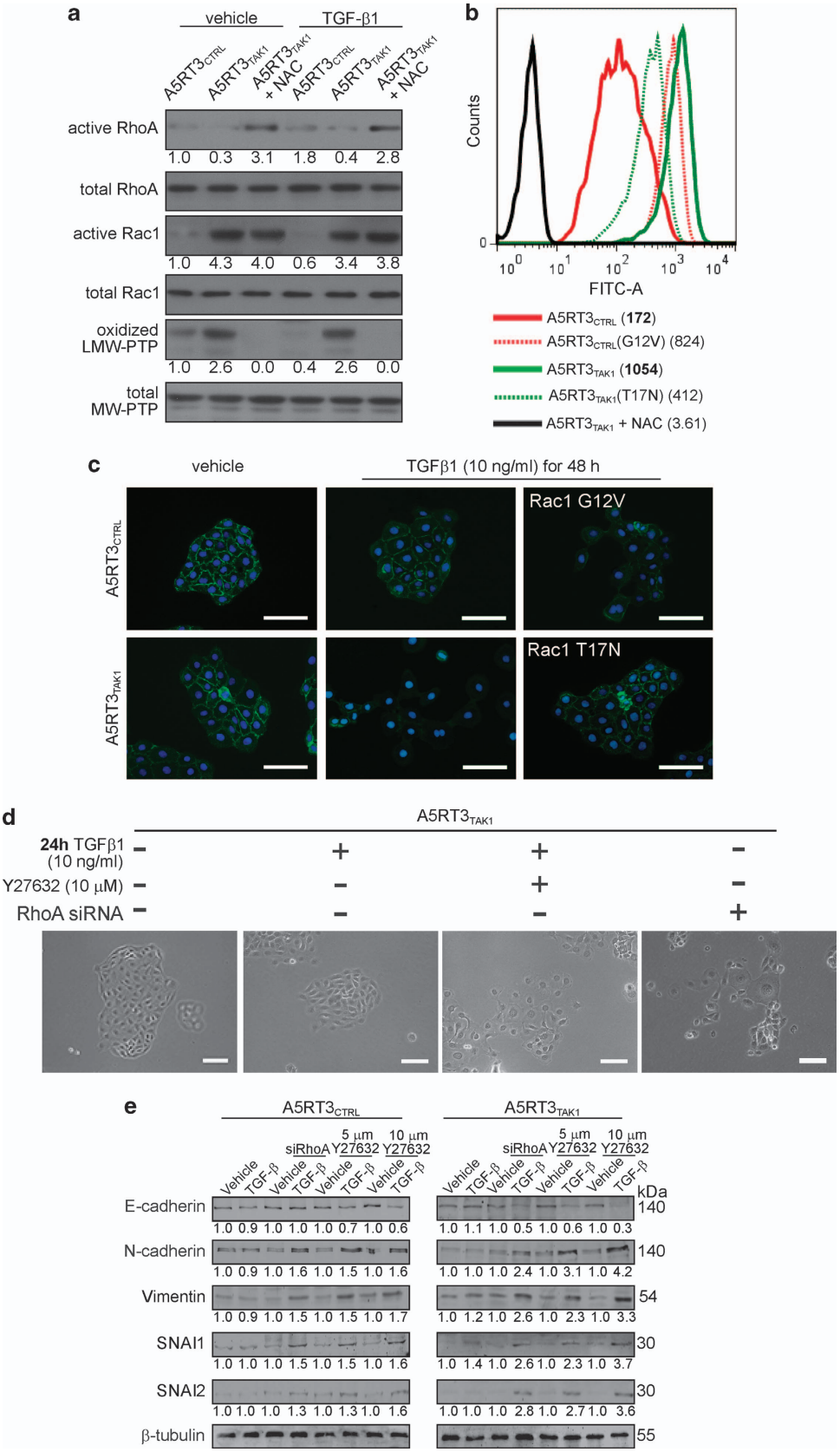
a
vehicle
TGF-β1
A5RT3CTRL
A5RT3TAK1
A5RT3TAK1 + NAC
active RhoA
1.0 0.3 3.1 1.8 0.4 2.8
total RhoA
active Rac1
1.0 4.3 4.0 0.6 3.4 3.8
total Rac1
oxidized LMW-PTP
1.0 2.6 0.0 0.4 2.6 0.0
total MW-PTP
b
Counts
FITC-A
A5RT3CTRL (172)
A5RT3CTRL(G12V) (824)
A5RT3TAK1 (1054)
A5RT3TAK1(T17N) (412)
A5RT3TAK1 + NAC (3.61)
c
vehicle
TGFβ1 (10 ng/ml) for 48 h
Rac1 G12V
Rac1 T17N
d
A5RT3TAK1
24h TGFβ1 (10 ng/ml)
Y27632 (10 μM)
RhoA siRNA
e
A5RT3CTRL
A5RT3TAK1
5 μm Y27632
10 μm Y27632
siRhoA
Vehicle
TGF-β
E-cadherin
1.0 0.9 1.0 1.0 1.0 0.7 1.0 0.6
1.0 1.1 1.0 0.5 1.0 0.6 1.0 0.3
N-cadherin
1.0 0.9 1.0 1.6 1.0 1.5 1.0 1.6
1.0 1.0 1.0 2.4 1.0 3.1 1.0 4.2
Vimentin
1.0 0.9 1.0 1.5 1.0 1.5 1.0 1.7
1.0 1.2 1.0 2.6 1.0 2.3 1.0 3.3
SNAI1
1.0 1.0 1.0 1.5 1.0 1.5 1.0 1.6
1.0 1.4 1.0 2.6 1.0 2.3 1.0 3.7
SNAI2
1.0 1.0 1.0 1.3 1.0 1.3 1.0 1.6
1.0 1.0 1.0 2.8 1.0 2.7 1.0 3.6
β-tubulin
kDa
140
140
54
30
30
55

Immunostaining and proximity ligation assay. Cells or tissue sections were fixed with 4% paraformaldehyde for 15 min, blocked and permeabilized in 3% BSA with 0.05% Triton-X for 1 h. Cells or tissue sections were incubated with either anti-vinculin (1 : 100), or monoclonal anti-E- cadherin (1 : 25), or anti-N-cadherin (1 : 25) or in anti-laminin-332 (1 : 50) in 0.3% BSA overnight at 4 °C. Secondary goat anti-rabbit Alexa Fluor 488 antibodies (1 : 200) in 0.2% BSA were added with incubation for 1 h at room temperature in the dark. Cells were then incubated with 1 : 50 dilution of Alexa Fluor 594 phalloidin (Molecular Probes, Eugene, OR, USA) in 2% BSA for 2 h and counterstained with DAPI (Vectashield, Burlingame, CA, USA). Between each step, slides were washed thrice with PBS. Immunofluorescent and phase-contrast images were taken using Nikon 80I Eclipse microscope equipped with a Nikon DS-SI1 camera, using a (20x/0.5) DIC objective and the NIS element D3.0 software with constant exposure and gain. Respective PLA assays were carried out as per manufacturer protocol (Olink Bioscience, St. Louis, MO, USA). Images were taken using Carl Zeiss (Thornwood, NY, USA) confocal microscope LSM 710meta using a Plan-Apochromat $\times$ 63/1.4 oil DIC objective, and ZEN 2009 LE software with constant exposure and gain. The resulting fluorescent spots were quantified using Duolink ImageTool (Olink Bioscience).

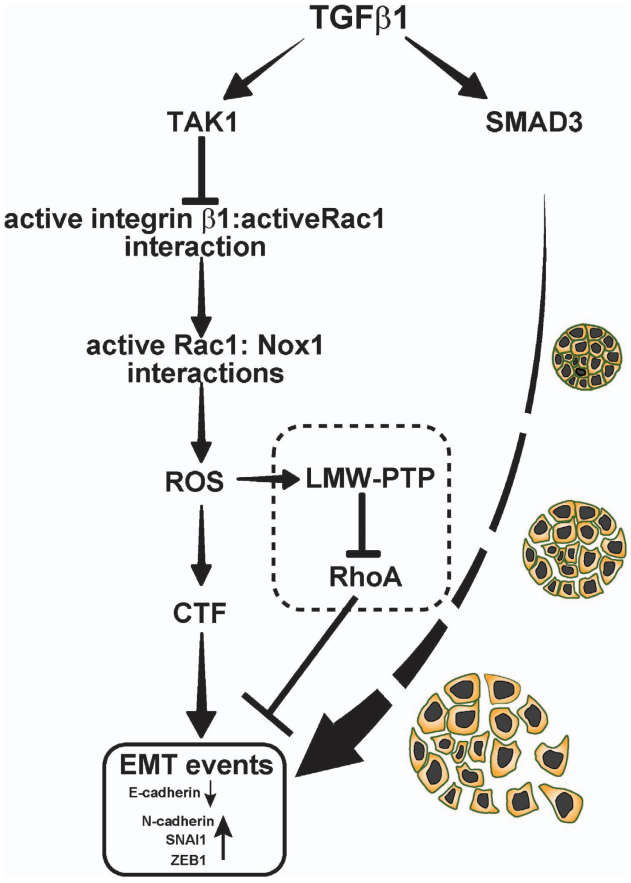

Figure 7 Proposed mechanism by which TAK1 inhibits TGFβ1-induced EMT. TAK1 likely counters the well-established TGFβ1-SMAD3 induction of EMT with the suppression of integrin expression and hence Rac1 activation. Rac activity otherwise promotes ROS production via the recruitment of Nox1, which oxidizes LMW-PTP and correspondingly inhibit RhoA activity, promoting EMT. Elevated ROS also leads to increased CTF, a characteristic of EMT progression

Flow cytometry. Cells were seeded and grown on 75 cm^2 culture flask (Corning, Tewksbury, MA, USA) until 50% confluence. Cells were then washed with PBS and incubated with 25 mM EDTA/PBS for 20 min. EDTA suspended cells were then spun down at 250 $\times$ g and fixed with resuspension in 4% paraformaldehyde for 20 min at room temperature. Fixed cells were spun down at 700 r.p.m. and washed with PBS twice through resuspension. Washed cells were then treated with anti-β1, β3, β4, β5, β7, α5β1 integrin antibodies, respectively at concentration (1 : 25) in 10% BSA and incubated at room temperature for 1 h. Cells were washed twice with PBS resuspension before incubation in secondary antibody conjugated with Alexa Fluor 488 at concentration (1 : 100) in 10% BSA at room temperature in the dark for 1 h. Stained cells were analyzed with Becton Dickinson (BD, Franklin Lakes, NJ, USA) LSRII flow cytometer. Analysis of flow cytometry results were performed with Flowjo software (Ashland, OR, USA). For ROS detection, cells were incubated with 10 μM CM-H2DCFDA (Invitrogen, Carlsbad, CA, USA) for 30 min at 37 °C prior to trypsinization and analysis by flow cytometry (LSRII from BD Biosciences). Results were analyzed by the Flowjo software. ROS was quenched with the addition of *N*-acetyl-L-cysteine (NAC) to a final concentration of 100 μM. CM-H2DCFDA-labeled cells were also imaged with the Nikon 80I Eclipse microscope equipped with a Nikon DS-SI1 camera, using a ($\times$ 20/0.5) DIC objective and the NIS element D3.0 software with constant exposure and gain.

Western blot analysis and detection of oxidized proteins. Cells (5×10^5) were lyzed in 100 μl lysis buffer (50 mM $Na_2H_2PO_4$, 250 mM NaCl, 1% Triton-X and 0.1% SDS). Equal amount of proteins were resolved by SDS-PAGE and transferred onto PVDF membrane (Millipore). Immunoblotting for β-tubulin was used to ensure equal loading of total proteins. The primary antibodies were used at dilutions of 1 : 4000 (TAK1), 1 : 2000 (NFκBp65), 1 : 2000 (phospho NFκBp65), 1 : 1000 (SMAD 3), 1 : 2000 (Fibronectin), 1 : 1000 (Vimentin) and 1 : 5000 (β-tubulin). Secondary antibodies were used at 1 : 5000 (anti-rabbit IgG), 1 : 10 000 (anti-mouse IgG) and 1 : 5000 (anti-goat IgG). All incubations were performed in 1 $\times$ TBS, pH 7.5, with 0.1% Tween-20 and either 5% fat-free milk (β-tubulin) or 5% bovine serum albumin (TAK1). Washing was performed with the same buffer without milk or BSA. The procedure to identify oxidized proteins (i.e. LMW-PTP) with biotin-NM was performed as earlier described.[39] Densitometry measurements of bands were performed with ImageJ software. The first band in each blot was given an arbitrary density of 1, and relative densities of the remaining bands were determined. Densitometry results of all individual bands are divided by those from tubulin and the ratio is presented as values below individual lanes.

Cell culture and transient transfection assay. Human embryonic kidney (HEK293-T) and human skin squamous cell carcinoma (A5RT3) cells were routinely maintained in DMEM and FBS (Hyclone, Pittsburgh, PA, USA). Transfection of $A5RT3_{CTRL}$ and $A5RT3_{TAK1}$ cells was carried out as per manufacturer's protocol (Fugene, Madison, WI, USA) with either plasmids expressing constitutive-active Rac1 G12V or dominant-negative Rac T17N.

Cell traction force (CTF) measurements. To measure cell contraction forces, cells were cultured on PDMS substrate embedded with fluorescent beads. Briefly, glass coverslips were cleaned by use of oxygen plasma before it was placed in a vacuum desiccator containing a small drop of 1H,1H,2H,2H-perfluorooctyltrichlorosilane for 30 min. Following which, the surface-treated coverslips were removed and 100 μl of diluted yellow–green FluoSpheres microspheres (0.2 μm, carboxylate-modified, 0.1 vol%,

Figure 6 Redox regulation of RhoA by Rac1 facilitates TGFβ1 induced EMT. (**a**) RhoA and Rac1 activities and LMW-PTP oxidation were compared with immunoblotting as respectively indicated. 10 ng/ml TGFβ1 and 100 μM of antioxidant NAC were used respectively for treatment duration of 48 h. (**b**) FACS analysis of tumor cells transfected with or without constitutive-active (G12V) and dominant-negative Rac1 (T17N). Antioxidant NAC-treated cells (100 μM) served as a negative control. Values shown indicate mean fluorescence intensity. (**c**) Representative images of E-cadherin (green/488 nm) immunostaining of tumor cells with respectively indicated treatments and transfection. Cell nucleus is stained with DAPI (blue). Scale bar, 100 μm. (**d**) Phase-contrast images of $A5RT3_{TAK1}$ cells with and without TGFβ1 induction were inhibited with Y27632 (10 μM) for 24 h or transfected with siRNA for RhoA. Representative phase-contrast images of treated cells. Scale bar, 100 μm. (**e**) Representative blots of EMT markers in TGFβ1-induced $A5RT3_{CTRL}$ and $A5RT3_{TAK1}$ treated with ROCK Y27632 or transfected with pooled siRNA for RhoA. Values shown with densitometry values indicated below respective lanes. Samples were normalized with tubulin as a loading control. Data represent means $\pm$ S.D.; $n = 3$

Molecular Probes) was added to the coverslips with the treated surface facing upwards. This step forms a monolayer of fluorescent beads on the coverslips. Thin film of PDMS were generated by placing 15 μl of PDMS mixture (before curing, 1 : 60 w/w of cross-linker to base ratio) on the fluorescent microspheres coated glass coverslips. One layer of Scotch tapes was applied as a spacer before putting the other bare glass coverslip on the top of fluorescent microspheres coated glass coverslips. The PDMS droplet was flattened under the weight of the upper coverslip. The entire assembly was left undisturbed for 5 min and then placed in 37 °C incubator overnight before carefully peeling off the upper bonded PDMS thin film with fluorescent microspheres on its top. Only samples with well-dispersed beads were used in the study. Substrates were UV sterilized for 30 min. As PDMS surface does not allow cells to adhere, the substrate was coated by incubation with human plasma derived fibronectin solution (50 μg/ml in 0.02 M acetic acid for thin coating) overnight to promote cell attachment. Coated substrates were rinsed with PBS, and stored in the dark at 4 °C prior to culture. 1×10^3 cells/inserts were seeded for 48 h under cell culture conditions. Cells were subsequently treated with 10 ng/ml TGFβ1 for 24 h before traction force measurement. All experiments were triplicated.

Calculation of CTFs was based on the elastic moduli of PA substrate and fluorescent beads displacements as previously described.[40] Spatial displacement of the beads was tacked by taking images of the fluorescent beads before and after cell trypsinization. The cell traction mapping was based on the DIC image of cells on PA substrate and the corresponding traction stress mapping in pseudocolor, which indicated regions of traction stresses (dark blue to light pink according to stresses from low to high). Briefly, the traction force at discrete point $\vec{f}_i$, located at the position (x_i, y_i) was calculated based on the following formulation: $\vec{u}_t(x,y) = \sum_{i=1}^{n} \vec{G}(x - x_i, y - y_i)\,\vec{f}_i$, where $\vec{G}$ denoted the Greens' tensor and $\vec{u}_t$ denoted the experimental displacements of fluorescent beads at position (x_i, y_i). The overall force of the cell (F) is an integral of the traction field magnitude over the area, $F = \iint \sqrt{T_x^2(x,y) + T_y^2(x,y)}\,dx\,dy$, where $T(x,y) = [T_x(x,y) + T_y(x,y)]$ is the continuous field of traction vectors defined at any spatial position (x,y) within the cell.

Transwell invasion assay. 5×10^4 cells were dispensed into the top chamber of transwell migration chambers (8 μm Millicell, Billerica, MA, USA; Hanging Cell Culture Inserts) loaded on a 6-well plate and allowed to attach overnight in cell culturing conditions. One thousand microliters of complete medium (supplemented with 10 ng/ml TGF-β1) was added to each of the underlying wells. For control wells, no TGF-β1 was supplemented. This construct was then incubated for 48 h. Following incubation, the inserts were washed with PBS and fixed with 1% glutaraldehyde for 10 min. The inserts were rinsed with PBS and subsequently stained in 0.1% crystal violet for 25 min. Cells were thoroughly rinsed with PBS after crystal violet staining. Cotton buds were used to swipe the upper surface of the transwell membrane, ensuring thorough removal of unmigrated cells. The inserts were then immersed in a 500 μl of 0.5% Triton-X solution dispensed in a clean 6-well plate and incubated overnight in the dark. The 6-well plate was sealed with parafilm tape to prevent evaporation. Absorbance of the 500 μl volume of 0.5% Triton-X at 595 nm was then measured using Nanodrop. The absorbance difference for the test and control wells were used as an index for the comparison of cellular migration.

Conflict of Interest

The authors declare no conflict of interest.

Acknowledgements. This work is supported by research grant from Ministry of Education (MOE 2010-T2-2-009) to NST. A5RT3 cell line was kindly provided by Dr Petra Boukamp of German Cancer Research Center DKFZ.

1. Mehlen P, Puisieux A. Metastasis: a question of life or death. *Nat Rev Cancer* 2006; **6**: 449–458.
2. Kalluri R, Weinberg RA. The basics of epithelial-mesenchymal transition. *J Clin Invest* 2009; **119**: 1420–1428.
3. Coussens LM, Werb Z. Inflammation and cancer. *Nature* 2002; **420**: 860–867.
4. Ikushima H, Miyazono K. TGFbeta signalling: a complex web in cancer progression. *Nat Rev Cancer* 2010; **10**: 415–424.
5. Zavadil J, Böttinger EP. TGF-beta and epithelial-to-mesenchymal transitions. *Oncogene* 2005; **24**: 5764–5774.
6. Zavadil J, Cermak L, Soto-Nieves N, Böttinger EP. Integration of TGF-beta/Smad and Jagged1/Notch signalling in epithelial-to-mesenchymal transition. *EMBO J* 2004; **23**: 1155–1165.
7. Reuter S, Gupta SC, Chaturvedi MM, Aggarwal BB. Oxidative stress, inflammation, and cancer: how are they linked? *Free Radic Biol Med* 2010; **49**: 1603–1616.
8. Toyokuni S, Okamoto K, Yodoi J, Hiai H. Persistent oxidative stress in cancer. *FEBS Lett* 1995; **358**: 1–3.
9. Lam CRI, Tan MJ, Tan SH, Tang MBY, Cheung PCF, Tan NS. TAK1 regulates SCF expression to modulate PKBα activity that protects keratinocytes from ROS-induced apoptosis. *Cell Death Differ* 2011; **18**: 1120–1129.
10. Omori E, Morioka S, Matsumoto K, Ninomiya-Tsuji J. TAK1 regulates reactive oxygen species and cell death in keratinocytes, which is essential for skin integrity. *J Biol Chem* 2008; **283**: 26161–26168.
11. Kim BG, An HJ, Kang S, Choi YP, Gao MQ, Park H *et al.* Laminin-332-rich tumor microenvironment for tumor invasion in the interface zone of breast cancer. *Am J Pathol* 2011; **178**: 373–381.
12. Imura J, Uchida Y, Nomoto K, Ichikawa K, Tomita S, Iijima T *et al.* Laminin-5 is a biomarker of invasiveness in cervical adenocarcinoma. *Diagnostic pathology* 2012; **7**: 105.
13. Marinkovich MP. Tumour microenvironment: laminin 332 in squamous-cell carcinoma. *Nat Rev Cancer* 2007; **7**: 370–380.
14. Hozumi Y, Kondo S, Shimoura T, Aso K. Human squamous cell carcinoma from skin: establishment and characterization of a new cell line (HSC-5). *J Dermatol* 1990; **17**: 143–148.
15. Mueller MM, Peter W, Mappes M, Huelsen A, Steinbauer H, Boukamp P *et al.* Tumor progression of skin carcinoma cells in vivo promoted by clonal selection, mutagenesis, and autocrine growth regulation by granulocyte colony-stimulating factor and granulocyte-macrophage colony-stimulating factor. *Am J Pathol* 2001; **159**: 1567–1579.
16. Motoyama T, Hojo H, Watanabe H. Comparison of seven cell lines derived from human gastric carcinomas. *Acta Pathol Jpn* 1986; **36**: 65–83.
17. Ihara Y, Inai Y, Ikezaki M. Alteration of integrin-dependent adhesion and signaling in EMT-like MDCK cells established through overexpression of calreticulin. *J Cell Biochem* 2011; **112**: 2518–2528.
18. Maschler S, Wirl G, Spring H, Bredow DV, Sordat I, Beug H *et al.* Tumor cell invasiveness correlates with changes in integrin expression and localization. *Oncogene* 2005; **24**: 2032–2041.
19. Omori E, Matsumoto K, Zhu S, Smart RC, Ninomiya-Tsuji J. Ablation of TAK1 upregulates reactive oxygen species and selectively kills tumor cells. *Cancer Res* 2010; **70**: 8417–8425.
20. Nimnual AS, Taylor LJ, Bar-Sagi D. Redox-dependent downregulation of Rho by Rac. *Nat Cell Biol* 2003; **5**: 236–241.
21. Aoudjit F, Vuori K. Integrin signaling in cancer cell survival and chemoresistance. *Chemother Res Pract* 2012; **2012**: 283181.
22. Mantovani A. Cancer: inflammation by remote control. *Nature* 2005; **435**: 752–753.
23. Sethi G, Shanmugam MK, Ramachandran L, Kumar AP, Tergaonkar V. Multifaceted link between cancer and inflammation. *Biosci Rep* 2012; **32**: 1–15.
24. Rahimi RA, Leof EB. TGF-beta signaling: a tale of two responses. *J Cell Biochem* 2007; **102**: 593–608.
25. Meulmeester E, Ten Dijke P. The dynamic roles of TGF-β in cancer. *J Pathol* 2011; **223**: 205–218.
26. Brandl M, Seidler B, Haller F, Adamski J, Schmid RM, Saur D *et al.* IKK(α) controls canonical TGF(ß)-SMAD signaling to regulate genes expressing SNAIL and SLUG during EMT in panc1 cells. *J Cell Sci* 2010; **123**: 4231–4239.
27. Valcourt U, Kowanetz M, Niimi H, Heldin CH, Moustakas A. TGF-beta and the Smad signaling pathway support transcriptomic reprogramming during epithelial-mesenchymal cell transition. *Mol Biol Cell* 2005; **16**: 1987–2002.
28. Huber MA, Azoitei N, Baumann B, Grünert S, Sommer A, Pehamberger H *et al.* NF-κB is essential for epithelial-mesenchymal transition and metastasis in a model of breast cancer progression. *J Clin Invest* 2004; **114**: 569–581.
29. Reuter S, Gupta S, Chaturvedi M, Aggarwal B. Oxidative stress, inflammation, and cancer: how are they linked? *Free Radic Biol Med* 2010; **49**: 1603–1616.
30. du Roure O, Saez A, Buguin A, Austin RH, Chavrier P, Silberzan P *et al.* Force mapping in epithelial cell migration. *Proc Natl Acad Sci USA* 2005; **102**: 2390–2395.
31. de Rooij J, Kerstens A, Danuser G, Schwartz MA, Waterman-Storer CM. Integrin-dependent actomyosin contraction regulates epithelial cell scattering. *J Cell Biol* 2005; **171**: 153–164.
32. Maschler S, Wirl G, Spring H, Bredow D, Sordat I, Beug H *et al.* Tumor cell invasiveness correlates with changes in integrin expression and localization. *Oncogene* 2005; **24**: 2032–2041.
33. Joshi A, Cao D. TGF-beta signaling, tumor microenvironment and tumor progression: the butterfly effect. *Front Biosci* 2010; **15**: 180–194.

34. Mueller MM, Fusenig N. *Tumor-Associated Fibroblasts and Their Matrix*. Springer Verlag, 2011.
35. Tlsty TD, Hein PW. Know thy neighbor: stromal cells can contribute oncogenic signals. *Curr Opin Genet Dev* 2001; **11**: 54–59.
36. Bhowmick NA, Chytil A, Plieth D, Gorska AE, Dumont N, Shappell S *et al.* TGF-beta signaling in fibroblasts modulates the oncogenic potential of adjacent epithelia. *Science* 2004; **303**: 848–851.
37. Cheng N, Bhowmick NA, Chytil A, Gorksa AE, Brown KA, Muraoka R *et al.* Loss of TGF-beta type II receptor in fibroblasts promotes mammary carcinoma growth and invasion through upregulation of TGF-alpha-, MSP- and HGF-mediated signaling networks. *Oncogene* 2005; **24**: 5053–5068.
38. Zhu P, Tan MJ, Huang RL, Tan CK, Chong HC, Pal M *et al.* Angiopoietin-like 4 protein elevates the prosurvival intracellular O2(-):H2O2 ratio and confers anoikis resistance to tumors. *Cancer Cell* 2011; **19**: 401–415.
39. Song BJ, Suh SK, Moon KH. A simple method to systematically study oxidatively modified proteins in biological samples and its applications. *Methods Enzymol* 2010; **473**: 251–264.
40. Dembo M, Wang YL. Stresses at the cell-to-substrate interface during locomotion of fibroblasts. *Biophys J* 1999; **76**: 2307–2316.

Supplementary Information accompanies this paper on Cell Death and Disease website (http://www.nature.com/cddis)